UNIVERSITY OF PARDUBICE
FACULTY OF TRANSPORT ENGINEERING

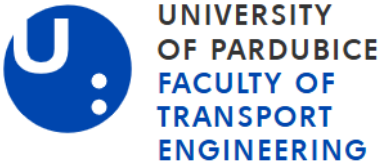

PROPOSAL OF A COMPUTER MODEL FOR SIMULATION OF CAR TIRES UNDER DYNAMIC LOADS

A summary of the Doctoral thesis submitted in fulfillment of the requirements
for the The degree of Doctor of Philosophy

2025 Ing. Sadjiep Tchuigwa Baurice Sylvain

Program of Study:
P0788D040002 - Transport Means and Infrastructure

Branch of study:
Transport Means

Dissertation Title:
Proposal of a computer model for simulation of car tires under dynamic loads

Author:
Ing. Sadjiep Tchuigwa Baurice Sylvain

Principal Supervisor:
Prof.Ing. Jan Krmela, Ph.D

Specialist Supervisor:
Ing. Jan Pokorny, Ph.D

The dissertation has arisen at the supervising:
Faculty of Transport Engineering, Department of Transport Means and Diagnostics.

Abstract

This study focuses on the modeling and simulation of car tires subjected to dynamic loads. As an essential part of the vehicle suspension system, tires ensure a proper transfer of loads to the ground and absorb rolling-induced vibration. In operating conditions, these loads are highly dynamic. However, the analysis of tires under these conditions has not been thoroughly explored in the literature. Therefore, the objective of this work is to address this gap. To achieve this, both the review of the experimental response of tire components in cyclic dynamic tests and the review of the existing tire models are conducted. Afterward, the methodology of a Finite element-based model that is consistent with material dynamic properties and dynamic load is proposed. An insightful strategy for the creation of the geometry, material parameter identification, choice of topology, boundary conditions, and solution scheme is proposed. In order to validate this model, simulations and experiments were conducted on a selected tire in static, dynamic and free vibration setups. The comparison of results, specifically the vertical deflection, contact area, mode shapes, and natural frequencies, demonstrates the model's accuracy. Furthermore, extensive responses such as steady-state rolling, vibration analysis, transient rolling, and steady-state dynamic were examined. Compared to static response, the results bring new findings regarding the effect of dynamic loads on the deformation and stress state in the tire. Moreover, this model is versatile and can be extended to investigate more responses, such as the acoustic, thermomechanical, aquaplaning and coupled noise, vibration, and harshness analyses. This work contributes to the advancement of the tire industry and highlights the significance of considering dynamic loads in the tire design phases for improving tire design, durability, and safety.

Keywords: Finite Element Method, Tire Simulation, Dynamic Load, Steady State Dynamic, Vibration, Transient Rolling.

Contents

1 Introduction

1.1 Context

Tires are essential components in both road and air transport, crucial for maintaining the integrity and stability of moving structures like cars, trucks, and aircraft. They transfer loads to the ground and absorb shocks from road imperfections, contributing to comfort, stability, and safety. There are many types of tires based on usage.

- Passenger and light truck tires: PT/LT;
- Bicycle tires;
- Motorcycle tires;
- Agricultural tires;
- Aero tires;
- Racing tires;
- Truck and bus tires.

Tires differ in design and bearing capacity, prompting ongoing research to enhance their performance based on various stresses and operating conditions. Despite advancements in tire technology, further optimization is essential due to resource use, environmental impact, and economic concerns. In today's world, where sustainability and performance demands are rising, there is a growing need for sophisticated simulation models to help manufacturers understand tire behavior and develop higher-performing products.

1.2 Research motivations

Given the dynamic loads that tires are subjected to throughout their service life, developing a computer model to simulate tires under these loads is

of paramount importance from both a scientific and industry perspective. Such a model will close the current gap in dynamic tire modeling, providing manufacturers with a more advanced modeling roadmap for product design and optimization. These motivations are highlighted in Figure 1.1.

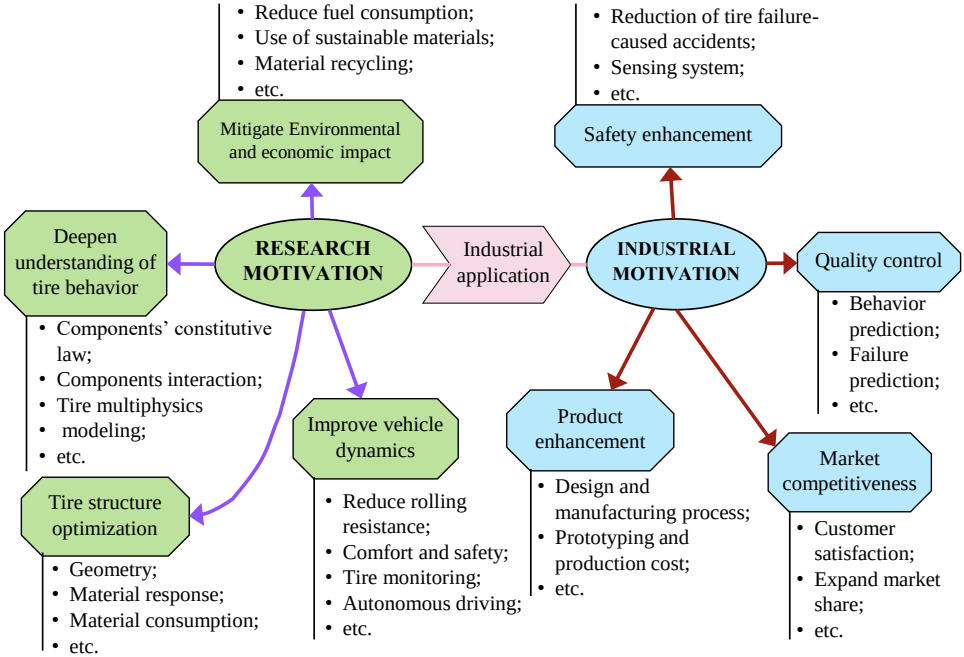

Figure 1.1: Motivation for the improvement of tire modeling.

1.3 Problem statement

Improving tire modeling and analysis for dynamic scenarios is crucial for understanding tire response and reducing the ecological impact of tire production. In recent years, the Finite Element Method (FEM) has become

a key technique for simulating various boundary value problems, including tire behavior. With advancements in computer technology, FEM effectively addresses both linear and nonlinear problems across multiple domains, including fluid, thermal, and mechanical simulations. The accuracy of FE models for tires depends on proper material laws, geometry definition, load application, boundary conditions, and solver choice. However, existing models struggle with dynamic loads due to inconsistencies in material behavior and high computational costs associated with required meshing. Still, FE models are significantly more powerful than analytical and semi-analytical tire models.

1.4 Research aim

Tires are subjected to dynamic loads, which must be considered during design to ensure safety and comfort. The dynamic response of a tire depends on the mechanical properties of its materials. Currently, no tire model effectively captures both reversible and irreversible material behaviors or allows dynamic simulation under varied conditions.

This thesis aims to **propose a material-consistent and computationally stable FEM-based model for simulating tires under dynamic loads**. The model will enhance the mechanical characterization of tire components and provide an efficient modeling strategy with optimal solver properties for accuracy and stability.
The aim of this thesis is to develop an innovative tire model that accurately predicts tire behavior under dynamic loads, addressing the limitations of existing models.

1.5 Research objective

In order to achieve the aim of this thesis, the following activities were carried out:

- **Literature review on tire models** (assumptions, inputs, limitations, purpose):

- **A detailed analysis of component behavior laws and identification of the parameters that influence the tire's dynamic response**:
- **Mechanical characterization, testing and calibration of tire parts**:
- **Development of a numerically stable modeling process**:
- **Experimental static and dynamic testing of a selected tire**:
- **Static, dynamic and vibration Validations of the numerical model based on experimental results**:
- **Simulation of various tire operational scenarios**:

1.6 Manuscript outline

The structure of this thesis summary is organized as follows:

Chapter 2 offers an overview of tire modeling, introducing tire functions and parts, along with a literature review on tire models. It particularly emphasizes finite element-based tire models, which inspire the current research.

In Chapter 3, methodology and the validation of numerical results against experimental results in static and dynamic setups are thoroughly presented in terms of deformation, contact pressure, and contact patch.

In Chapter 4, findings, model limitations, future recommendations and concluding remarks are discussed and highlighted.

2 Presentation and state of art on tire models

Tires in their current design are the outcome of decades of engineering improvement and evolution. Their complex structure has evolved ever since in terms of material and design techniques. The aim of this chapter is first to present the tire structure and its characteristics. Secondly, to review the literature on tire simulation models and identify their limitations.

2.1 Definition and functions

The tire is a composite structure made from elastomers and reinforcements, ensuring effective contact and load transfer between the vehicle and the pavement. Tires are vital in various applications, particularly in aircraft landing gears, trucks, and passenger vehicles, with specific designs tailored to each use. This thesis focuses exclusively on car tires.

There exist two distinct designs of car tires, namely radial tires and bias tires. While radial tires are made with respectively 0° and 90° oriented plies toward the longitudinal direction of the tire, bias tires are made with plies unaligned following the longitudinal and transversal direction.

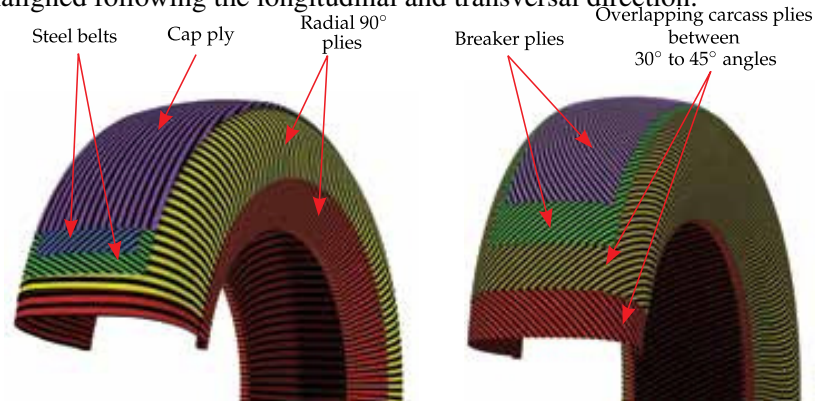

Figure 2.1: radial tire casing (left) versus bias tire casing (right) [1].

Tire components:

A cross-section on a tire reveals a combination of different components (see Figure 2.2) of various properties. It is this complex design that makes the tire such a special structure, as each of its components is judiciously positioned and chosen.

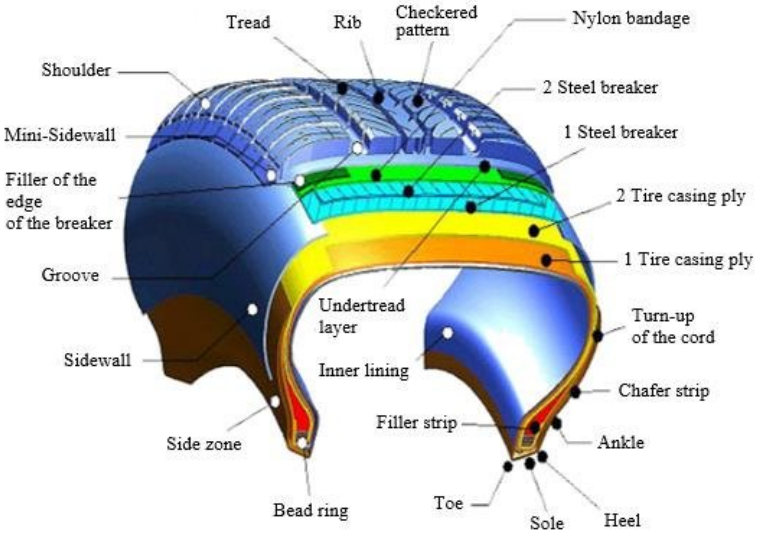

Figure 2.2: Tire casing parts [2].

2.2 Literature review

2.2.1 Review of experimental data from tire component testing:

The response of a tire is closely linked to its components. We will analyze laboratory tests but identifying parameters can be challenging due to the costs of testing equipment and specimens.

Steel cords:

Steel cords operate mainly in the lower stress-strain region, adhering to Hooke's law without plastic deformation, as indicated by tensile tests from

Korunović et al. [3] and Wei and Olatunbosun [4]. Consequently, a simple uniaxial tensile test suffices to determine Young's modulus (E_{steel}) and Poisson's ratio (ν_{steel}), which are key parameters.

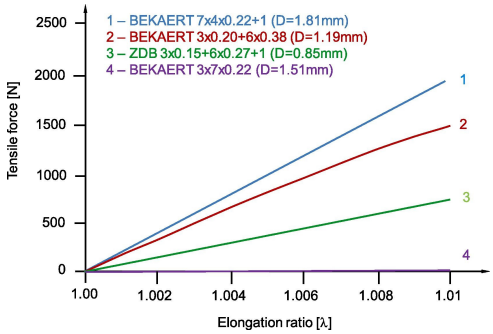

Figure 2.3: Tensile test results of several steel cords [3].

Rubber compounds:

Rubber compounds used for tire making exhibit in uniaxial tensile test, a very large deformation [5] whilst still remaining in the elastic region as depicted in Figure 2.4.

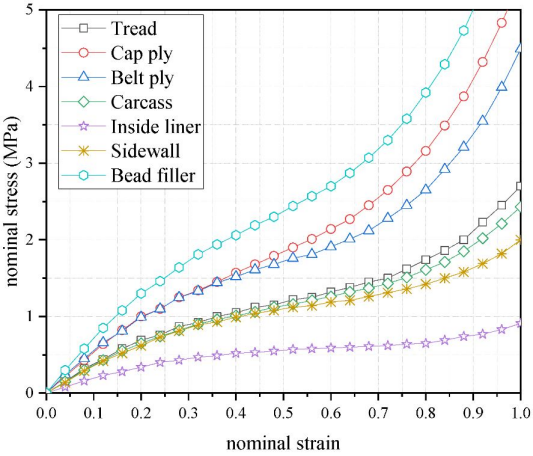

Figure 2.4: Rubber compounds response in uniaxial tensile test [6].

In a cyclic tensile test [7], they rather depict a combination of hysteresis and stress softening response, as shown in Figure 2.5.

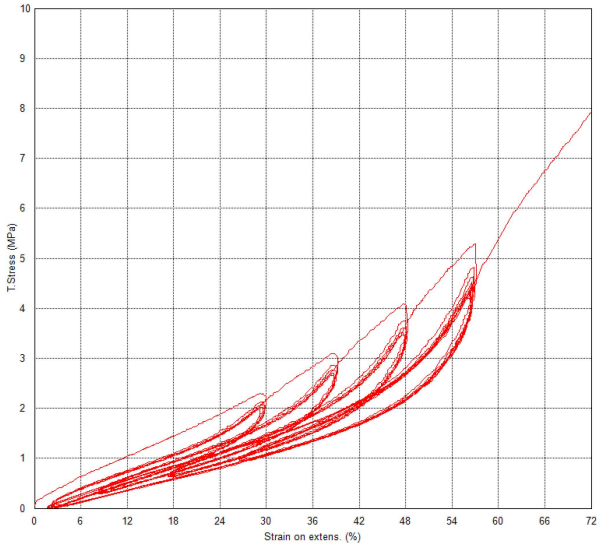

Figure 2.5: Rubber compounds response in uniaxial tensile cyclic test [7].

Significant research has investigated stress softening in filled rubber from material and structural perspectives. Materially, Mullins [8] demonstrated that fillers like silica and carbon black improve strength and abrasion resistance. Structurally, two models have emerged: the micromechanical model, initiated by Bueche [9], focuses on the breakage of molecular bonds due to stress softening, with refinements from others including Govindjee and Simo [10]. The macromechanical model, developed by Ogden and Roxburgh [11], applies damage concepts from Lemaitre [12] to explain Mullins damage. The primary model for the Mullins effect during loading-unloading cycles comes from Dorfmann and Ogden [13], while Göktepe [14] introduced a unified micro-macromechanical approach to describe rubber behavior. However, for computational simplicity, the micromechanical approach is disregarded in this thesis.

Textile cords:

Laboratory cyclic tensile tests on tire textile cords by [7] and others [15], [16] show a slightly hyperelastic response under monotonic load and minimal viscoelastic+Mullins damage under cyclic tests, as illustrated in Figure 2.6. Compared to rubber compounds, the hysteresis loops of textile cords are negligible, allowing for their treatment as linear elastic materials for computational simplicity.

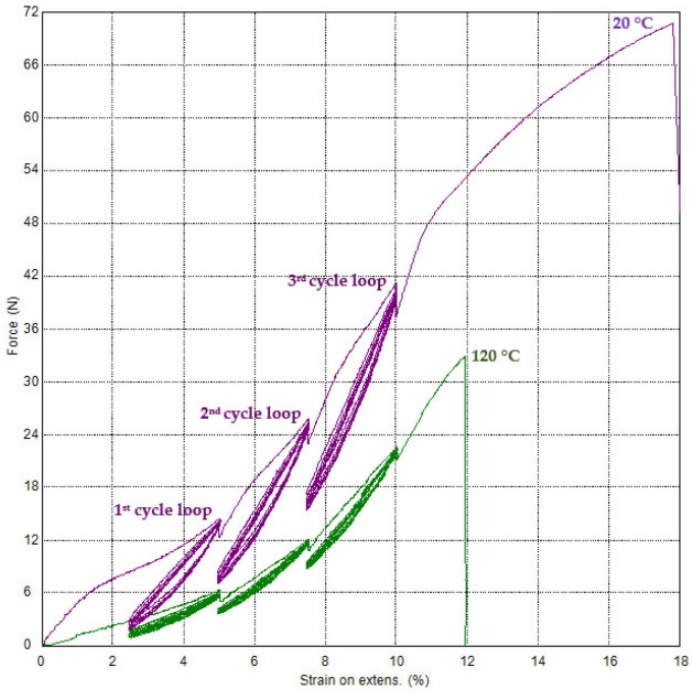

Figure 2.6: Stress-strain dependence of PA66 in cyclic tensile test at 20°C and 120°C [7].

2.2.2 Literature review on tire models

In the literature, tire models are ranked into three categories, namely empirical, semi-theoretical, and purely theoretical models as depicted in Figure 2.7. Only a few models are explored in this section.

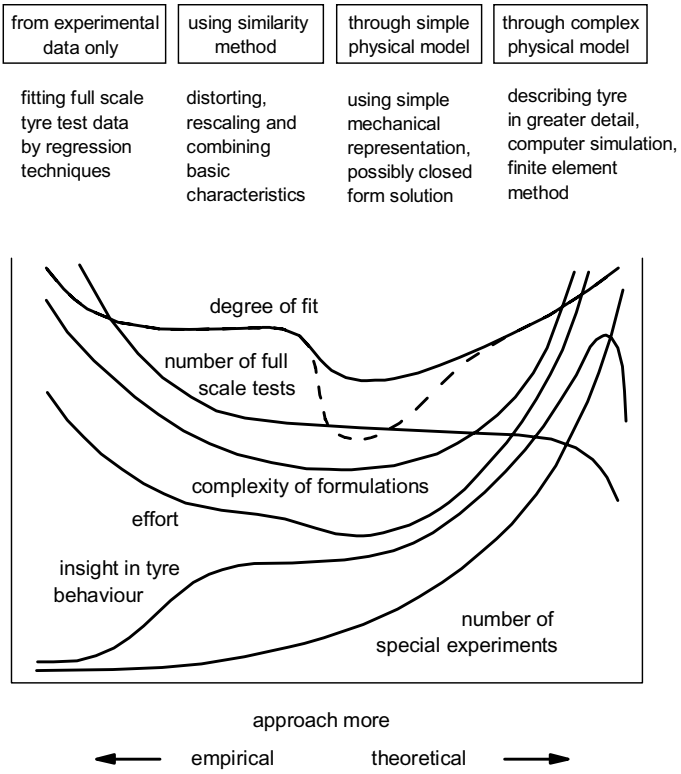

Figure 2.7: Types of tire modeling approaches [17].

Empirical tire models

Among empirical tire models, we have:

- The Magic Formula tire model developed by Pacejka [17], which mathematically describes tire handling based on slip ratio, applied force, slip angle, and camber angle.
- The Fiala tire model [18], which represents the tire belt as a thin circular disk in point contact with the road, utilizing three formulas related to slip rate, slip angle, vertical force, and friction coefficient.

Semi-empirical tire models

To address the lack of physical considerations in empirical models, several semi-empirical models have been developed:

- The Brush Tire Model [19] analyzes tire steady state rolling using flexible bristles to model the tread attached to a rigid carcass.
- The brush-string model [17] improves upon the original by incorporating string elements for tire carcass stiffness, enhancing contact patch analysis and local deformation during maneuvers.
- The Flexible Ring Tire Model [20] features a deformable tread represented by elastic springs, contrasting with rigid ring models.

Theoretical tire models

Theoretical tire models are valued for their precision and capability to address complex physical issues. Numerical methods like the Finite Element Method (FEM) facilitate research by incorporating realistic factors. Below are notable studies in this field:

- Alkan et al. [21] developed a static tire model using hyperelastic rubber and linear isotropic laminate layers, validated through tests on various cleat types on a flat surface.
- Golbakhshi and Namjoo [22] explored the impact of air pressure, speed, temperature, and axial load on tire rolling resistance using a hyperelastic material model, with static load applied in a ramp manner.
- Phromjan and Suvanjumrat [23] examined how the number and position of belt layers affect the performance of non-pneumatic tires through Finite Element Analysis, using a visco-hyperelastic material model.

- Mohsenimanesh et al. [24] constructed a truck tire model to analyze off-road tire-road interaction with linear elastic rubber and orthotropic reinforced layers.
- Fontaine et al. [25] created a model incorporating linear orthotropic belt layers and hyperelastic rubber to evaluate static load behavior.
- Wei and Olatunbosun [4] proposed a dynamic model for predicting tire cornering performance and relaxation length in rolling conditions, combining visco-hyperelastic rubber with linear elastic reinforcements.
- Tielking [26] designed a shell model to assess how design variables affect the deformation of a four-ply bias tire under vertical load.
- Noor [27] introduced nonlinear shell-based tire strategies with contact constraints, effectively predicting mechanical and thermal responses during tire-pavement interaction.

2.3 Research gap

Numerous material constitutive laws exist for rubber, often approximated as linear or hyperelastic. However, experimental tests show a more complex behavior: **visco-hyperelastic with Mullins effect**, which affects tire performance during rolling, cornering, and braking under varying load frequencies. Accurate tire performance relies on damping properties to absorb dynamic excitations. Most existing mechanical models only consider static loads, ignoring dynamic conditions. This thesis aims to **propose a FEM-based model to simulate tires under dynamic loads**, incorporating the dynamic properties of tire components for improved accuracy.

3 Simulation, results and validation of the model

In this chapter, we have proceeded with the implementation and experimental validation of the computer model proposed in this thesis. The structure of the chapter is as follows: First, Section 3.1, the finite element model (FEM) of the selected tire was introduced. Next, in Section 3.2, we utilized this model for simulations and validated it against experimental results obtained from laboratory tests.

3.1 Methodology

3.1.1 Model presentation

In this study, we analyze the Matador $165/65\mathrm{R}13\ 77\mathrm{T}\ \mathrm{MP}16$ tire, designed for passenger vehicles. It has a width of $165\mathrm{mm}$, an aspect ratio of 65%, and fits a rim of $330.2\mathrm{mm}$ in diameter. The tire's construction (see Figure 3.1) includes rubber components, two layers of steel cords, one layer of textile cord, and one ply layer. Its load index (LI) is $412\ \mathrm{Kg}$, with a maximum inflation pressure of $300\mathrm{kPa}$.

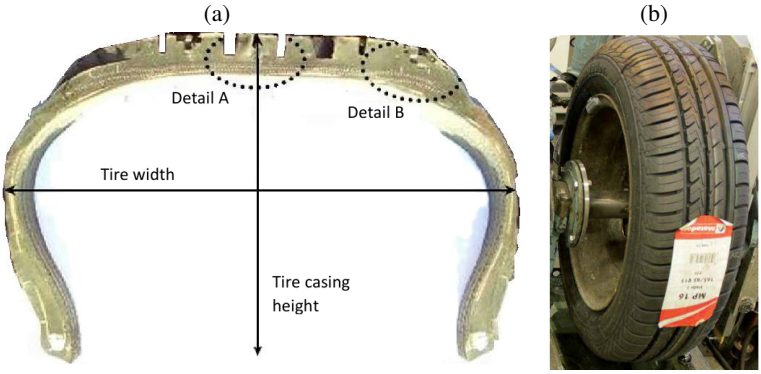

Figure 3.1: Cross-section and 3D view on $165/65\mathrm{R}13\ 77\mathrm{T}\ \mathrm{MP}16$ tire.

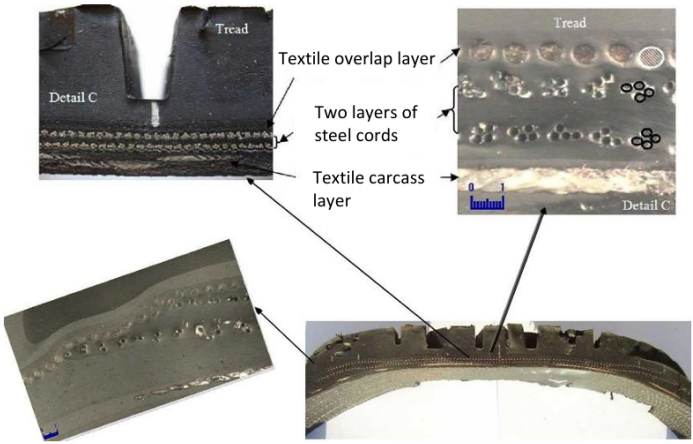

Figure 3.2: Details of casing.

This tire consists of various rubber-like components, including the tread, sidewall, rim cushion (bead rubber), inner liner, and rubber for both steel-cord and textile-cord belts. The carcass angle is set at zero degrees, with steel cords at 23 degrees and textile overlaps at 90 degrees. A detailed view of these components can be seen in Figure 3.1.

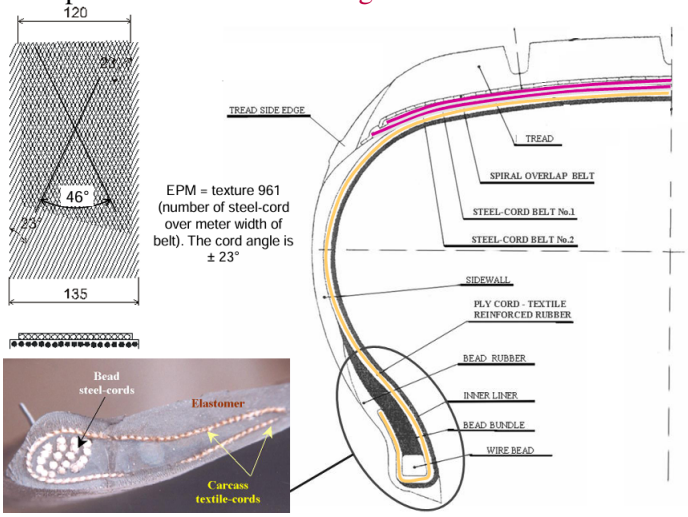

Figure 3.3: Tire casing parts.

Besides the internal components of the tire casing, the rolling surface of this tire is designed with patterns to ensure stability in adverse rolling conditions, as shown in Figure 3.1(b).

3.1.2 Topology

The tire topology creation began with scanning the cross-section (see Figure 3.3), which was imported into AUTOCAD for sketching the layers and components. This sketch was then imported as a *.stp* file into ABAQUS to create a 2D axisymmetric cross-section. Rubber compounds were modeled with CGA3RH and CGA4RH elements, while reinforcements were modeled using SFMGAX1 surface elements. Finally, the 3D mesh of the tire was generated following the workflow in Figure 3.4.

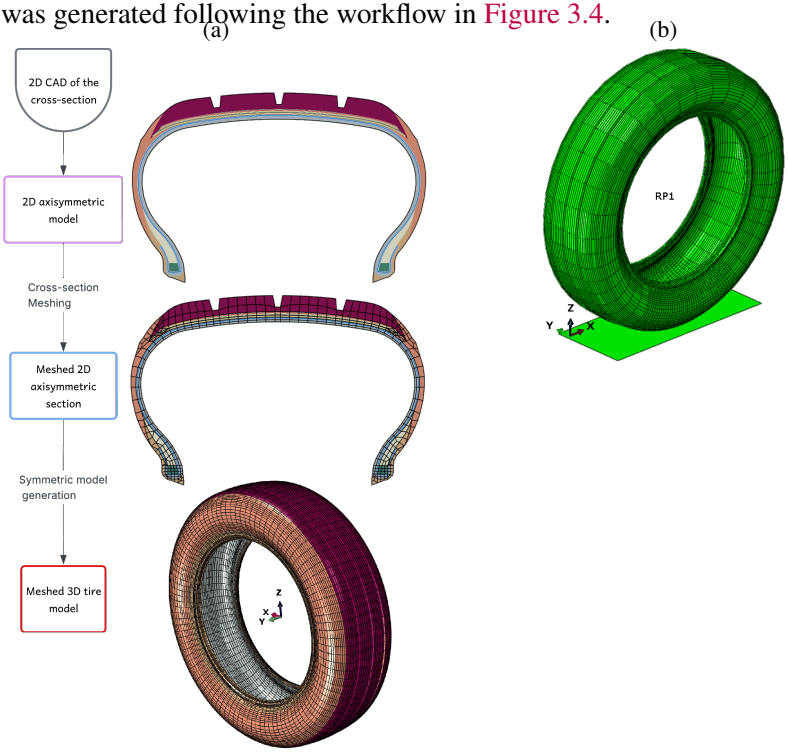

Figure 3.4: (a) Tire modeling workflow. (b) Full 3D model for static analysis.

Surface-to-surface interaction modeled the contact between the tread surface (slave) and the road (master). In addition to the sectorized mesh topology (mesh *Type 2*), we also used an equally spaced sector mesh (*Type 1*).

3.1.3 Material properties

Input parameters, such as mechanical properties, are crucial in a finite element model. Experimental tests were performed on tire specimens. Rubber compounds underwent uniaxial tensile cyclic testing per ISO 37:2017, following the method in Krmela et al. [28] (see P10). Reinforcements, including steel and textile cords, were tested according to ASTM standards. After calibration with the given constitutive laws, the material properties were obtained and listed in Table 3.1, Table 3.2 and Table 3.3.

Table 3.1: Reinforcement material propeties.

Tire parts	E [MPa]	ν	$\varnothing$ [mm]	spacing [mm]	ρ [Kg/m^3]	Orientation [°]
Steel cords	160 000	0.30	0.60	1.09	5 600	23
Textile cap cords	3 400	0.40	0.69	0.9	950	90
Carcass	11 000	0.40	0.49	1.0	950	0
Bead	180 000	0.30	/	/	6 800	/

Table 3.2: Material properties of rubber compounds.

	Hyperelasticity				**Mullins effect**		
Parts	ρ [Kg.m^{-3}]	C_{01} [MPa]	C_{10} [MPa]	D_1 [MPa^{-1}]	r	m	β
Bead filler	801	-0.111	1.945	0.01097	10.25	0.8	1.25
Inner liner	801	0.109	0.259	0.05471	13.2	0.92	1.91
Rim cushion	801	0.692	0.0371	0.01894	8.36	1.08	2.52
Sidewall	801	0.532	0.065	0.03372	21.67	0.732	1.151
Tread	801	0.417	0.519	0.02151	17.37	1.19	1.05
Rubber[a]	801	0.328	0.119	0.04504	12.18	0.987	2.349
Rubber[b]	801	0.548	0.112	0.03051	26.94	1.03	1.102
Rubber[b]	801	0.638	0.284	0.02183	21.615	0.89	3.25

Table 3.3: Material properties of rubber compounds.

	Viscoelasticity: Prony series					
Parts	g_1	τ_1 [s]	g_2	τ_2 [s]	g_3	τ_3 [s]
Bead filler	0.00498	0.000265	0.1082	258.341	0.207	1786.528
Inner liner	0.0835	0.0321	0.264	128.341	0.172	2185.35
Rim cushion	0.217	0.0108	0.3897	108.836	0.0428	1152.719
Sidewall	0.0137	0.512	0.124	204.534	0.0587	2431.25
Tread	0.0207	0.012	0.315	317.654	0.0934	1386.241
Rubber[a]	0.0125	3.464	0.137	148.26	0.223	2124.201
Rubber[b]	0.0231	0.0231	0.225	187.054	0.127	1350.16
Rubber[c]	0.0364	0.726	0.135	238.780	0.0605	2057.35

[a] rubber part for steel cords.
[b] rubber part for textile cap cords.
[c] rubber part for carcass cords.

We should note that the orientation of steel cords in Table 3.1 is with respect to the local axis 2. Since angles were defined using local axis 1 in axisymmetric, we calculate the angle as $90° - 23° = 67°$.

3.1.4 Analysis flowchart

With all ingredients for our model ready, we ran simulations and conducted various tests to validate it.

- Quasi-static validation on the static adhesor.
- Quasi-static and dynamic validation on the dynamic adhesor.
- Modal vibration validation.

After validation, we analyzed tire response using the proposed model during steady-state rolling, post-steady-state vibration, random vibration, and transient rolling. The workflow for these analyses is summarized in Figure 3.5.

Figure 3.5: Workflow for model deployment and validation.

3.2 Results and Validation of the model

3.2.1 Quasi-static state validation using static adhesor setup:

Experimental setup

The laboratory test for this study was conducted on the static adhesor (see Figure 3.6)located within the Alexander Dubček University of Trenčín. On this machine, it is possible to test passenger tires with rim ranging from R13 to R18 and with a maximum width of 235 mm.

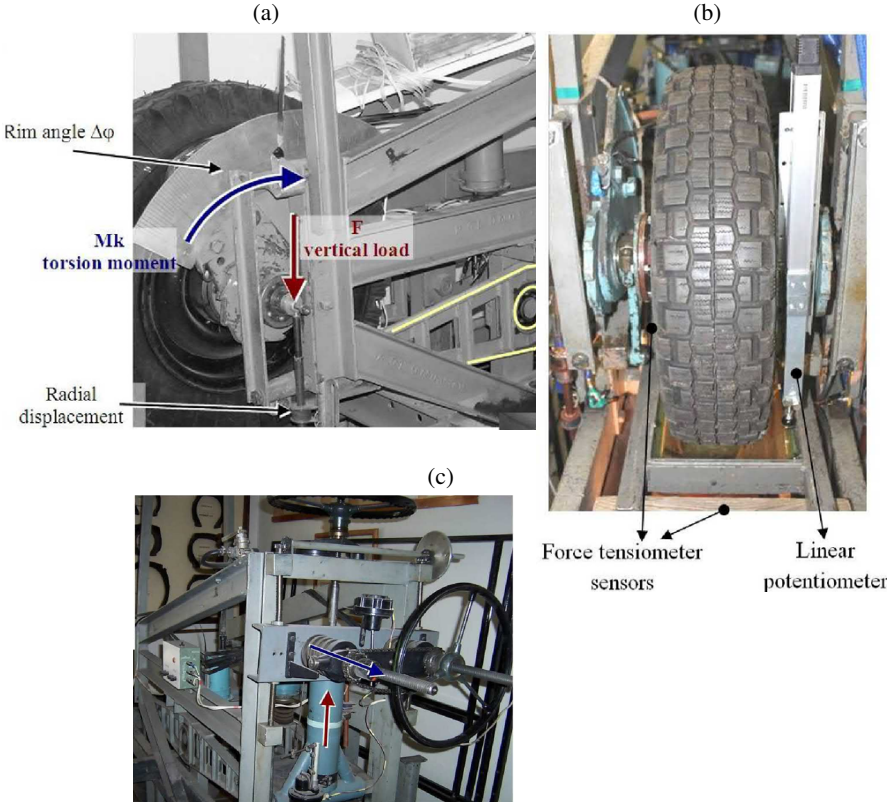

Figure 3.6: Views of the static adhesor [29].

Experimental data were collected following the experimental setup outlined on the static adhesor at different inflation pressures (180kPa and 250kPa) and under a vertical load varying from 0 to 125% of the LI. We recall that for the selected tire, $LI = 412$ Kg, which corresponds to a load of 4041.72 N.

Results and validation

The simulation with the proposed model was efficient and cost-effective. The total CPU time for this analysis was approximately 10 minutes.

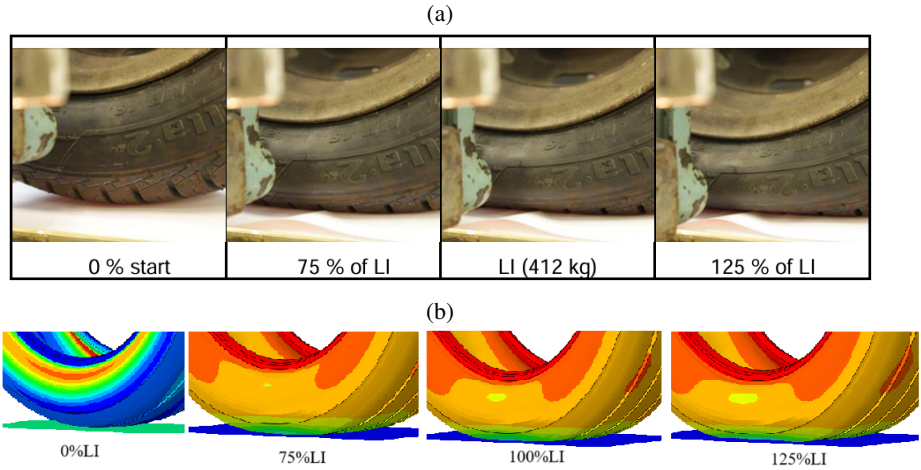

Figure 3.7: Visualization of tire deformation during vertical static loading. (a) Experiment and (a) FE model.

Comparison between u_z^{exp} and u_z^{FEM}

After executing the jobs with the created Abaqus input file, the dependence of force versus deflection at the node $RP1$ (wheel center) was retrieved and plotted in a Figure 3.8 alongside the curve of force versus displacement measured experimentally.

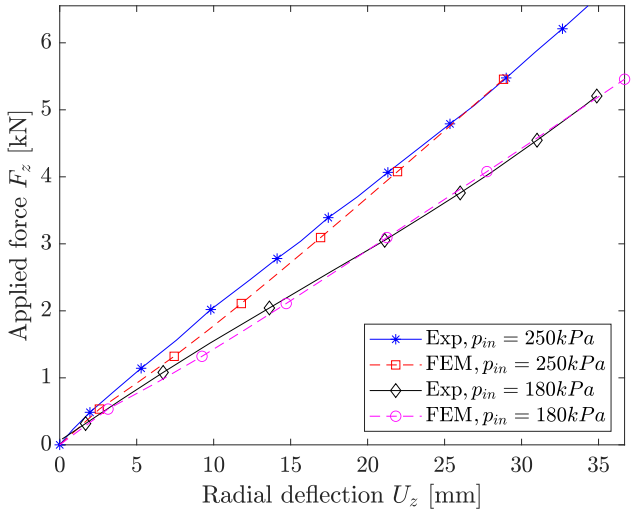

Figure 3.8: Numerical and experimental results of the applied load F_z versus the radial deflection u_z on the static adhesor.

Now, talking quantitatively about the data from Figure 3.8, Table 3.4 compares the experimental and numerical values obtained for an inflation pressure of 180 and 250 kPa, considering a load F_z equal to 100% of the load index. Here, the absolute relative error (%) is utilized as the metric for this comparison.

Table 3.4: Comparison of radial deformation between the numerical model and experiment at 100%LI

p_{in} [kPa]	Radial deformation U_z (in mm) at 100%LI		
	Simplified model	Experimental	Relative error (%)
180	27.75	27.00	2.78
250	21.76	21.50	1.16

We observe that the resulting relative error is less than 5% in both cases. Consequently, the proposed model is accurate with respect to the prediction of the radial deflection on the static adhesor.

Comparison of the contact patch from experiments and FEM results

During the experimental tests with an inflation pressure of 250kPa, the contact patch on the ground was captured at $100\%\text{LI}$ using a thin film, and the resulting dimensions were also measured. In addition, the contact shape was recorded as output from the numerical model on both the simplified and the complex models. The visualization of these contact patches is displayed in Figure 3.9(a).

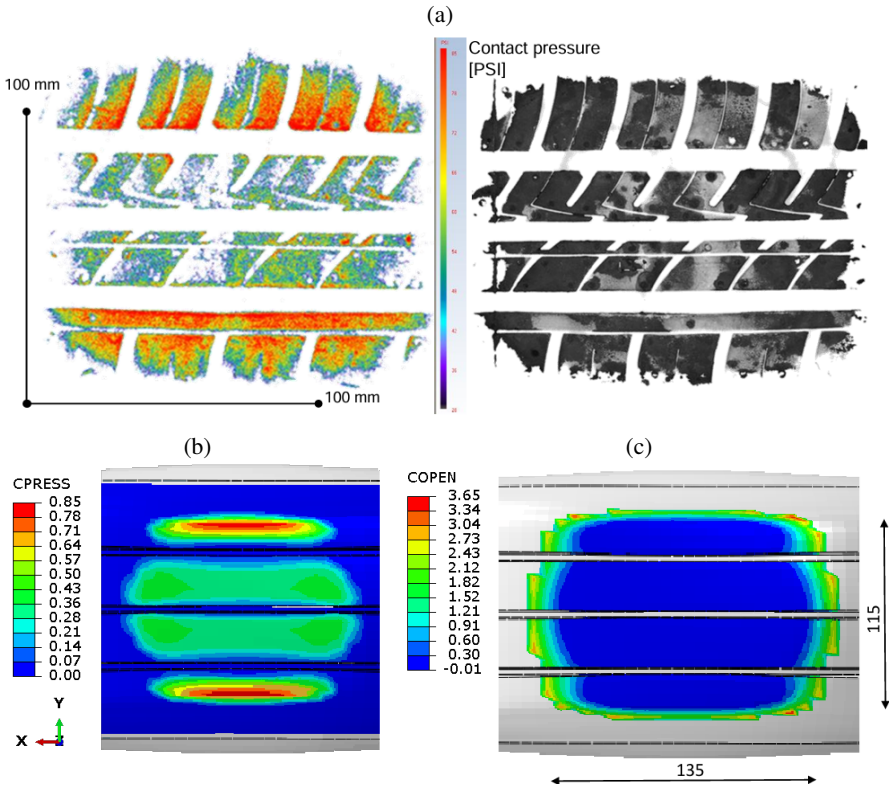

Figure 3.9: Visualization of contact stress and contact patch from FE model and expriment at 100%LI. (a) Experiment, (b) and (c) are respectively the contact pressure and contact patch from FE model.

The examination of the contact patches reveals a similarity in the distribution of the contact imprints, which is especially noticeable towards the edges. Additionally, it is observed that the effective contact surface is larger in the FE model. This is evident because, in this model, the actual shape of the grooves has been simplified. The resulting contact areas are summarized in the Table 3.5.

Table 3.5: Comparison of contact area between the numerical (simplified) and experimental results at 100%LI

p_{in} [kPa]	Contact area $A_{contact}$ (in mm^2) at 100%LI		
	Simplified model	Experimental	Relative error (%)
180	11840	11820	0.2
250	11200	10125	10.6

At an inflation pressure of 180 [kPa], the experimental and numerical contact areas match at a 100% load index (LI). However, the finite element (FE) model shows a contact area about 10% larger than the experimental measurement, which is expected due to the smoother surface of the tire model compared to a real tread pattern. At this pressure and a radial force (F_z) of 100% LI, the tire is considered under-inflated.This indicates that the effective contact area is concentrated on the longitudinal edges of the tire.

A more accurate contact area can be obtained for the case with $p_{in} = 250$kPa by using instead the tire model with real tread pattern. The resulting contact area is summarized in Table 3.6.

Table 3.6: Comparison of contact area between the numerical model and experiment at 100%LI

p_{in} [kPa]	Contact Area (in mm^2) at 100%LI		
	Complex model	Experimental	Error(%)
250	10015	10125	1.1

The obtained contact patch is displayed in Figure 3.10.

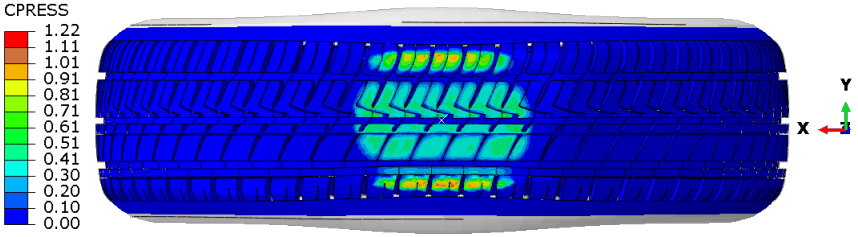

Figure 3.10: Contact patch obtained on the tire with tread pattern.

Comparison of the radial stiffness from experiment and FEM

Based on the dependence of the applied force on the deflection, it is possible to compute the radial stiffness k_z.

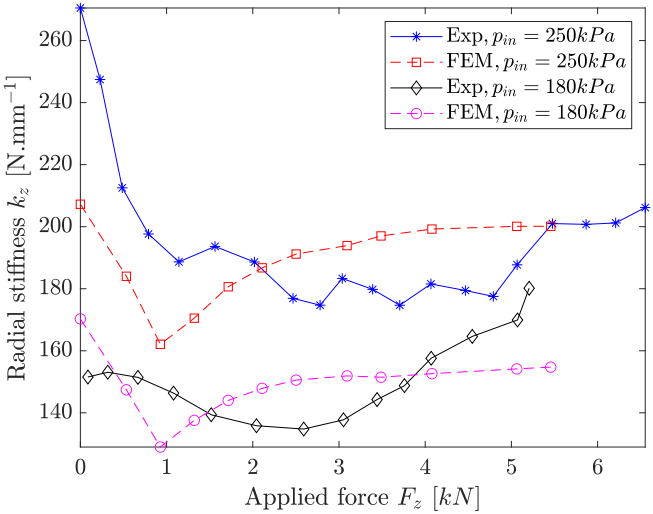

Figure 3.11: Numerical versus experimental radial stiffness k_z.

For vehicle dynamic analysis, it is a common practice to estimate a single value of k_z rather than having it dependent on the applied force. According to ČSN 63 1511 standard[30], this value is given as

$$k_z = \frac{F_{z,125\%LI} - F_{z,75\%LI}}{u_{z,125\%LI} - u_{z,75\%LI}} \tag{3.1}$$

The main drawback of this formula is that it does not take into account some features related to the loading process. Thus, Krmela and Michal [31] alleviated this limit with the formula below

$$k_z = \frac{F_{z,100\%LI} - F_{z,60\%LI}}{u_{z,100\%LI} - u_{z,60\%LI}} \tag{3.2}$$

Therefore, using the formula in Eq.(3.2), we can compare the experimental and numerical values in Table 3.7.

Table 3.7: Comparison of radial stiffness between the numerical model and experiment

p_{in} [kPa]	Radial stiffness k_z (in [N.mm^{-1}])		
	Simplified model	Experimental	Relative error (%)
180	151.29	153	1.11
250	194.97	185	5.38

In view of the results, it can be seen that the absolute relative error is acceptable.

3.2.2 Quasi-static and dynamic state validation using the dynamic adhesor setup:

Static testing on the dynamic adhesor (see Figure 3.12) involves using a stationary drum (of diameter $\phi_{drum} = 1.705m$), which remains at zero speed, onto which the tire is moved through a force-driven sequence. This sequence is regulated by a hydraulic system, which is monitored on the control board

located in the control room. The outcome of this testing procedure measures the radial deformation in response to the applied force.

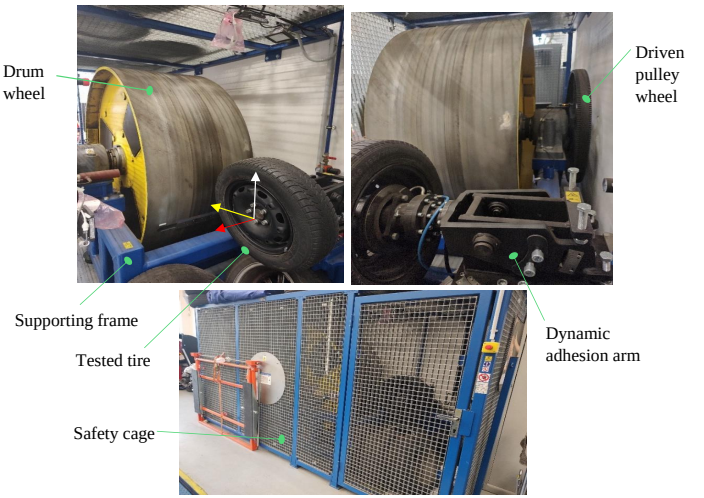

Figure 3.12: View on the dynamic adhesor.

A schematic illustration of this testing setup is shown in Figure 3.13.

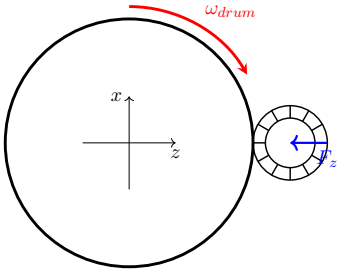

Figure 3.13: Schematic view of tire testing on dynamic adhesor: drum on the left and tire on the right.

Three inflation pressures $p_{in} \in \{160\text{kPa}, 250\text{kPa}, 300\text{kPa}\}$ were considered, and the applied load varying monotonically such that $F_z \in [0, 135\%\text{LI}]$. The drum was modeled as a rigid surface.

Static test validation: At zero speed

The simulation was completed very quickly, taking approximately 10 minutes for each inflation level. The experimental and numerical results are shown in Figure 3.14.

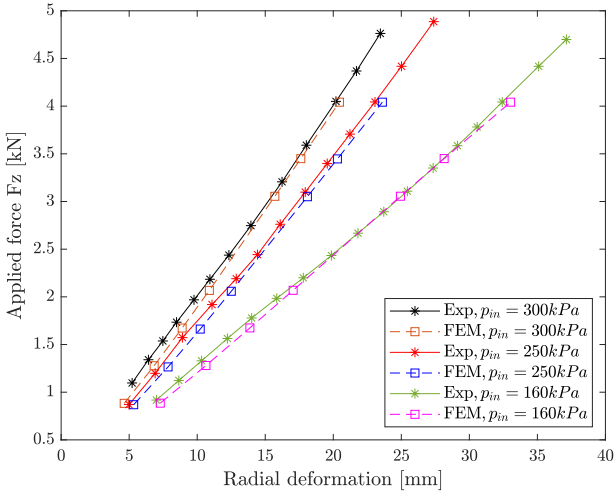

Figure 3.14: Numerical and experimental results of the applied load F_z versus the radial deflection u_z at zero speed on the dynamic adhesor.

It can be seen from the curves that the numerical model predicts the response of the tire to vertical loads very well. More concretely, at $100\%LI$, the absolute error is less than 5% as summarized in Table 3.8.

Table 3.8: Comparison of radial deflection on dynamic adhesor at 300kPa inflation and 0 $\mathrm{Km.h^{-1}}$ speed.

p_{in} [kPa]	Radial deformation $\mathrm{U_z}$ (in mm)		
	Simplified model	Experimental	Relative error (%)
160	33.03	32.40	1.9
250	23.60	23.05	2.4
300	20.45	20.15	1.5

Dynamic test validation: with a rotating drum

The radial test on the dynamic adhesor was conducted using a drum rotating at $V = 120$ Km.h^{-1}, corresponding to an angular speed of $\omega_{drum} = \frac{V}{R_{drum}} = 19.55$ rad.s^{-1}. Experimental and numerical results are shown in Figure 3.15.

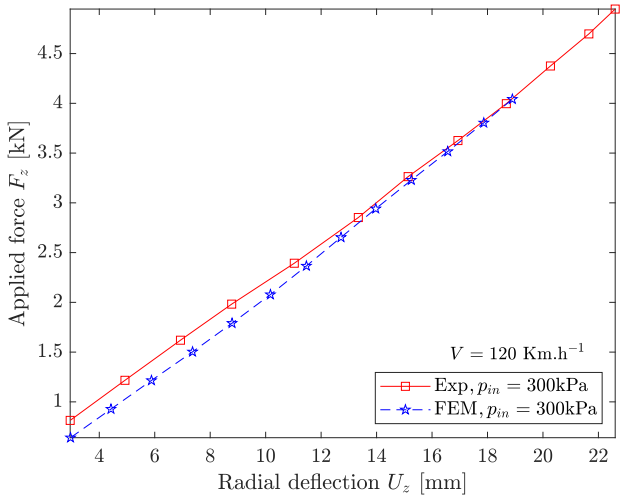

Figure 3.15: Numerical and experimental results of the applied load F_z versus the radial deflection u_z on the dynamic adhesor at a speed of 120 Km.h^{-1}.

We observe that both results are very similar, despite a small difference at low force. The comparison at $100\%LI$ is reported in Table 3.9.

Table 3.9: Comparison of the radial deflection on the dynamic adhesor at 300kPa inflation and 120 Km.h^{-1} speed.

p_{in} [kPa]	Radial deformation U_z (in mm) under 100%LI		
	Simplified model	Experimental	Relative error (%)
300	18.90	18.87	0.16

The absolute error at low force ($F_z < 45\%LI$) is about 7%, while

it drops to less than 2% under higher loads. The increased relative error at lower forces is likely due to temperature effects from the tire's friction against the rotating drum and inaccuracies in the hyperelastic material model. However, the relative error remains acceptable. In conclusion, the model effectively predicts tire deformation under dynamic load.

3.2.3 Modal analysis

The purpose of this section is to analyze the natural vibration of the unloaded tire under an inflation pressure of $250\mathrm{kPa}$ and use experimental results to validate the accuracy of simulation results.

Experimental setup

Under laboratory conditions, the tire was inflated to $250\mathrm{kPa}$ and mounted on the test rig, as shown in Figure 3.16.

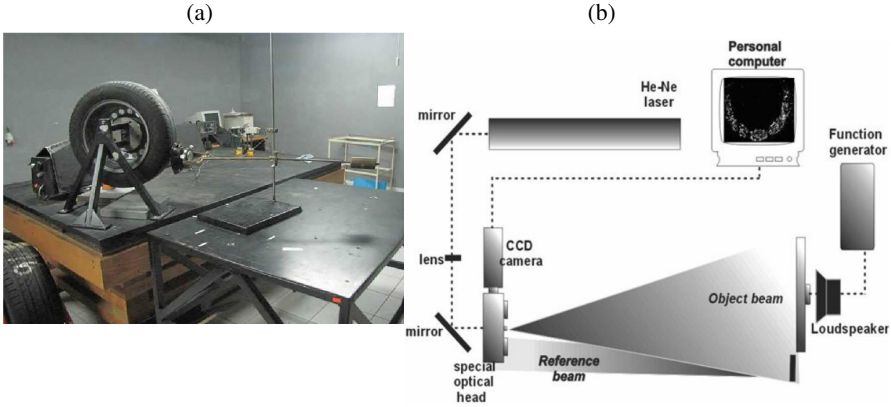

Figure 3.16: Experimental setup for measuring modal vibration of unloaded tire. (a) View on the experimental setup (b) Apparatus and its components [32].

An Electronic Speckle Pattern Interferometer (ESPI) system was used to measure tire surface deformation and modal frequencies and shapes.

FEM model

The workflow exploited for this analysis is highlighted in Figure 3.17.

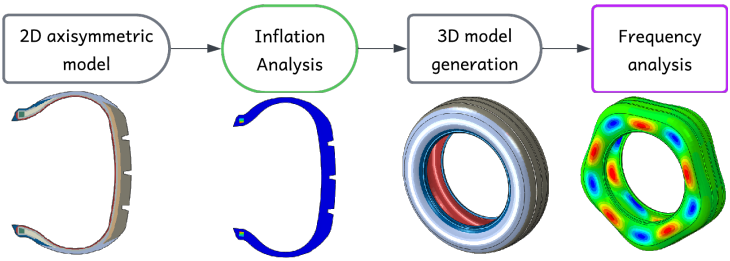

Figure 3.17: Flowchart of the Modal analysis

Results and discussions:Validation of modal analysis

After obtaining frequencies and mode shapes from the proposed FEM model and experiments, we compare the results. The ESPI system captures modal vibration shapes and frequencies, which we organized into radial and axial mode shapes for comparison with the simulation results. Table 3.10 displays the computed and measured axial vibration modes.

Table 3.10: Comparison of out-of-plane mode shapes between the FE and experiment results

Name	Experiment		FEM		Error
	f_{Exp}[Hz]	Modeshape	f_{FEM}[Hz]	Modeshape	
A2	120	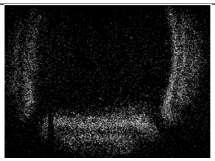	107.34	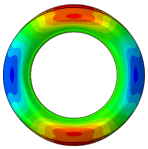	9.72
A3	179	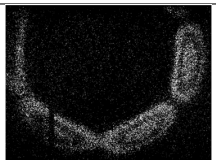	166.92	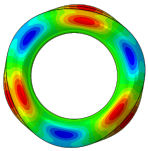	6.75

Table 3.11 compares radial modes from FEA results with those measured.

Table 3.11: Comparison of in-plane shapes between the FE and experiment results

Name	Experiment		FEM		Error (%)
	f_{Exp}[Hz]	Mode shape	f_{FEM}[Hz]	Mode shape	
R2	136	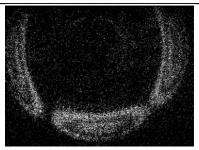	129.36	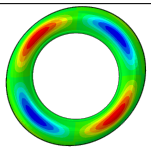	4.88
R3	166	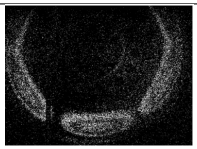	160.00	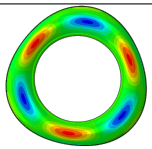	3.61
R4	188	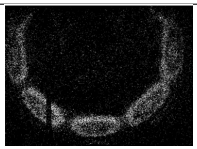	190.17	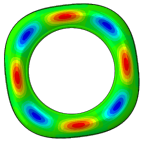	1.15
R5	208		220.27	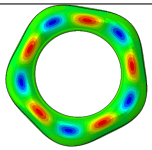	5.89
R6	239	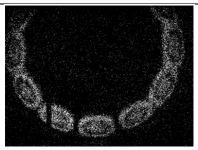	248.93	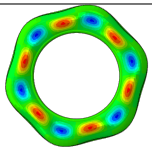	4.15

Besides the axial mode A1 and A2, the relative error between calculated and measured modes is less than 6%. Thus, we conclude that the accuracy of the model is verified.
The analysis of the mode shapes reveals that the vibration patterns exhibit

great similarity across the FE model and experiment. Specifically, the number of vibration lobes or fields remains consistent for each mode, underscoring a strong correlation between both results.

4 Conclusions

Summary

This study developed a finite element model to simulate car tires under dynamic loads. After reviewing existing literature, we created a model that reflects the dynamic responses of tire components and real-world load conditions. We proposed a multistage modeling methodology detailing inputs like topology, mechanical properties, loads, and implementation in ABAQUS.

The model simulation of the Matador $165/65\mathrm{R}13\ 77\mathrm{T}\ \mathrm{MP}16$ tire closely matched experimental data under static and dynamic loads. Validation included static and dynamic adhesion setups (with and without speed) and a free vibration setup, measuring displacement, contact area, natural frequencies, and mode shapes. The maximum relative error between experimental and numerical results was less than 5%, except for axial natural frequencies, which were about 9%.

In industrial practices, tire vibrational response characterization often focuses on natural frequencies, assuming failures occur only during resonance. However, our analysis of a dynamic periodic load using steady-state dynamic analysis showed that failure can also happen in resonance-free modes. We observed that the tire's center deflection under small amplitude load impulses was significantly larger than under static loads, highlighting the need to expand beyond traditional resonance assessments.

In addition, in explicit transient analysis of the same tire rolling on an uneven surface has brought out a key finding:

- A sudden acceleration can cause tire resonance, leading to blowouts and structural failure while rolling.
- In rolling conditions, dynamic deformations and stresses from road contact are crucial for tire stability and durability.

The model significantly improves efficiency, reducing computational time for footprint analysis from 69 minutes in the preliminary version to just

10 minutes in the final version with a similar mesh size. However, transient, steady-state rolling, and dynamic footprint analyses still take several hours on medium-sized meshes due to high computational costs. A proposed solution is a vectorized algorithm that leverages the computer's architecture to reduce computation time. This work enhances tire modeling, aiding engineers in understanding tire dynamics for safer, more efficient car tires.

Future work

Future work could concentrate on validating the steady-state rolling analysis and incorporating material failure criteria to simulate and experimentally validate tire failure mechanics.

Recommendations

Based on the findings from this work, the following recommendations are provided:

- The axisymmetric approach for tire geometry and topology is optimal due to its computational robustness and accuracy, as shown by experimental and numerical results.
- More accurate results in dynamic analysis can be obtained by incorporating thermal effects, specifically through thermo-mechanical analysis.
- To reduce mesh size, it's advisable to partition the cross-section into smaller regions before meshing.
- The addition of Mullins damage enhances material response prediction and improves numerical scheme convergence.
- For modal extraction, the rebar-continuum approach better accounts for reinforcement's mechanical contribution.
- Using advanced phenomenological material models like Ogden, Yeoh, or Gent can yield more accurate results.

References

[1] Kenda Americana Tire and Wheel, "Difference between radial and bias trailer tires," Reynoldsburg, Tech. Rep., 2018, p. 20. [Online]. Available: https://americanatire.com/differences-between-radial-and-bias-tires/.

[2] V. Ievleva and V. Hammatova, "Analysis of technical textiles used for automobile tires," *Bulletin of Kazan Technological University*, vol. 20, no. 16, pp. 64–8, 2017.

[3] N. Korunović, C. Fragassa, D. Marinković, N. Vitković, and M. Trajanović, "Performance evaluation of cord material models applied to structural analysis of tires," *Composite structures*, vol. 224, p. 111 006, 2019, ISSN: 0263-8223. DOI: 10.1016/j.compstruct.2019.111006.

[4] C. Wei and O. A. Olatunbosun, "The effects of tyre material and structure properties on relaxation length using finite element method," *Materials Design*, vol. 102, pp. 14–20, 2016, ISSN: 0264-1275. DOI: 10.1016/j.matdes.2016.04.014.

[5] X. Yang, O. A. Olatunbosun, and E. O. Bolarinwa, "Materials testing for finite element tire model," *SAE Technical Papers*, vol. 3, no. 1, pp. 211–220, 2010, ISSN: 26883627. DOI: 10.4271/2010-01-0418.

[6] Y. Liu, Z. Qian, C. Liu, and Q. Huang, "Investigation on hydroplaning behaviors of a patterned tire on a steel bridge deck pavement," *Applied Sciences*, vol. 11, no. 22, 2021, ISSN: 2076-3417. DOI: 10.3390/app112210566.

[7] J. Krmela, M. Michna, Z. Růžička, V. Krmelová, and A. Artyukhov, "Cyclic testing of polymer composites and textile cords for tires," *Polymers*, vol. 15, no. 10, 2023, ISSN: 2073-4360. DOI: 10.3390/polym15102358.

[8] L. Mullins, "Softening of rubber by deformation," *Rubber Chemistry and Technology*, vol. 42, no. 1, pp. 339–362, Mar. 1969, ISSN: 1943-4804. DOI: 10.5254/1.3539210.

[9] F. Bueche, "Molecular basis for the mullins effect," *Journal of Applied Polymer Science*, vol. 4, no. 10, pp. 107–114, 1960.

[10] S. Govindjee and J. Simo, "Transition from micro-mechanics to computationally efficient phenomenology: Carbon black filled rubbers incorporating mullins' effect," *Journal of the Mechanics and Physics of Solids*, vol. 40, no. 1, pp. 213–233, 1992.

[11] R. W. Ogden and D. G. Roxburgh, "A pseudo–elastic model for the Mullins effect in filled rubber," *Proceedings of the Royal Society of London. Series A: Mathematical, Physical and Engineering Sciences*, vol. 455, no. 1988, pp. 2861–2877, Aug. 1999, ISSN: 1364-5021. DOI: 10.1098/rspa.1999.0431.

[12] J. Lemaitre, *A course on damage mechanics*. Springer science & business media, 2012.

[13] A. Dorfmann and R. Ogden, "A constitutive model for the Mullins effect with permanent set in particle-reinforced rubber," *International Journal of Solids and Structures*, vol. 41, no. 7, pp. 1855–1878, Apr. 2004, ISSN: 00207683. DOI: 10.1016/j.ijsolstr.2003.11.014.

[14] S. Göktepe, *Micro-macro approaches to rubbery and glassy polymers: Predictive micromechanically-based models and simulations*. 2007.

[15] W. Wang, S. Yan, and Y. Zhao, "Numerical and experimental studies of a radial truck tire with tread pattern," *Simulation*, vol. 91, no. 11, pp. 970–979, 2015, ISSN: 17413133. DOI: 10.1177/0037549715608434.

[16] Y. Li, C. Liu, Y. Sun, Y. Li, C. Xu, and M. Xie, "Modeling Methods and Simulation Analysis of Radial Tire with Different Tread Patterns," vol. 9, no. 1, pp. 20–30, 2020.

[17] H. Pacejka, *Tire and vehicle dynamics*. Elsevier, 2005. DOI: 10.1016/C2010-0-68548-8.

[18] E. Fiala, "Lateral forces on rolling pneumatic tires," *Zeitschrift VDI*, vol. 96, no. 29, pp. 973–979, 1954.

[19] H. Dugoff, P. S. Fancher, and L. Segel, "Tire performance characteristics affecting vehicle response to steering and braking control inputs," Highway Safety Research Institute, The University of Michigan, Tech. Rep., 1970.

[20] M. Gipser, "Ftire–the tire simulation model for all applications related to vehicle dynamics," *Vehicle System Dynamics*, vol. 45, no. S1, pp. 139–151, 2007.

[21] V. Alkan, S. Karamihas, and G. Anlas, "Finite element modeling of static tire enveloping characteristics," *International Journal of Automotive Technology*, vol. 12, pp. 529–535, 2011.

[22] H. Golbakhshi and M. Namjoo, "An efficient numerical scheme for evaluating the rolling resistance of a pneumatic tire," vol. 5, pp. 1009–1015, Jul. 2015.

[23] J. Phromjan and C. Suvanjumrat, "Belt layer effects on non-pneumatic tire performance by finite element analysis," in *Recent Advances in Manufacturing Engineering and Processes*, R. K. Agarwal, Ed., Singapore: Springer Nature Singapore, 2023, pp. 149–157, ISBN: 978-981-19-6841-9.

[24] A. Mohsenimanesh, S. Ward, and M. Gilchrist, "Stress analysis of a multi-laminated tractor tyre using non-linear 3d finite element analysis," *Materials & Design*, vol. 30, no. 4, pp. 1124–1132, 2009. DOI: https://doi.org/10.1016/j.matdes.2008.06.040.

[25] M. Fontaine et al., "Static in-tire circumferential strain signature using rayleigh-scattering fiber optic technology: Preliminary results," in *Transport Research Arena TRA 2020*, Helsinki, Finland: Proceedings of 8th Transport Research Arena TRA 2020, 2020, pp. 149–157. [Online]. Available: https://univ-eiffel.hal.science/hal-04486233.

[26] J. T. Tielking, "A Finite Element Tire Model," *Tire Science and Technology*, vol. 11, no. 1, pp. 50–63, Jan. 1983, ISSN: 0090-8657. DOI: 10.2346/1.2150979.

[27] A. K. Noor, "Nonlinear analysis and modeling of tires. final report, 12 september 1990-31 december 1995," Virginia University, Tech. Rep., May 1996. [Online]. Available: https://www.osti.gov/biblio/382988.

[28] J. Krmela, V. Krmelova, M. Gavendova, A. Bakosova, A. Kasperovich, and B. S. Sadjiep Tchuigwa, "Methods for determining the physico-mechanical properties of polymers," in *-2020*, 2020, pp. 168–171.

[29] J. Krmela, *Experiments and Computational Modelling of Tires: Textbooks for university students*. Zborov, Czech Republic: Jan Krmela, 2020, ISBN: 978-80-270-9020-4.

[30] C. S. Agency, "Standard: Testing of tyres. determination of static radial stiffness and static tyre radius," International Organization for Standardization, Czech Republic, Standard, Jan. 2000.

[31] J. Krmela and P. Michal, "Determination of radial stiffness of tire from experiments on the static test device called static adhesor," *Metallurgical Journal (Hutnické listy)*, vol. 7, no. 1, pp. 81–84, 2012, ISSN: 0018-8069.

[32] P. Koštial, Z. Jančíková, D. Bakošová, J. Valícek, M. Harnicarova, and I. Špička, "Artificial neural networks application in modal analysis of tires," *Measurement Science Review*, vol. 13, Oct. 2013. DOI: 10.2478/msr-2013-0040.

Author's publications

List of author's published and in review results in relation to PhD thesis

Journal papers: published

P1 **B. S. Sadjiep Tchuigwa**, J. Krmela, J. Pokorny, V. Krmelová, and P. Jilek, "Vectfem: A generalized matlab-based vectorized algorithm for the computation of global matrix/force for finite elements of any type and approximation order in linear elasticity," Zeitschrift für angewandte Mathematik und Physik, vol. 75, no. 4, p. 150, 2024, ISSN: 1420-9039. DOI: 10.1007/s00033-024-02293-w, **WoS Q2 (SCOPUS Q1/D2) Jimp**.

P2 **B. S. Sadjiep. Tchuigwa**, J. Krmela, and J. Pokorny, "A literature review on tire component requirements," Perner's Contacts, vol. 16, p. 6, Dec. 2021, ISSN: 1801-674X, DOI: 10.46585/pc.2021.2.1740.

Journal papers: in review

P3 **B. S. Sadjiep. Tchuigwa**, J. Krmela, J. Pokorný and V. Krmelova, "Numerical and experimental validation of car tire testing on the static and dynamic adhesors: an enhanced tire model with Mullins damage," under review in Composites Communications.

P4 **B. S. Sadjiep. Tchuigwa**, J. Krmela, J. Pokorný and V. Krmelova, "Dynamic loads and their Impact on the Vibration Behavior of Car Tires: A Numerical and Experimental Study," under review in Discover Materials.

Conference proceedings : published

P5 **B. S. Sadjiep Tchuigwa**, J. Krmela, and J. Pokorny, "Toward detailed modeling of tires with linear elastic rubber compounds using finite

element method," IOP Conference Series: Earth and Environmental Science, vol. 1380, no. 1, p. 012 018, Aug. 2024, ISSN: 1755-1315. DOI: 10.1088/1755-1315/1380/1/012018. (indexed in Scopus).

P6 **B. S. Sadjiep Tchuigwa**, J. Krmela, and J. Pokorný, "A numerical study of the influence of the choice of rubber material behavior on the static response of tires," IOP Conference Series: Earth and Environmental Science, vol. 1380, no. 1, p. 012 019, Aug. 2024, ISSN: 1755-1315. DOI: 10.1088/1755-1315/1380/1/012019. (indexed in Scopus).

P7 **B. S. Sadjiep Tchuigwa**, J. Krmela, J. Pokorny, and V. Krmelová, "Improved and vectorised matlab-based algorithms for serial and parallel implementation of finite element method in linear elasticity," in Proceeding of the 23rd International Scientific Conference on Engineering for Rural Development, Jelgava, May 2024, pp. 1–6. DOI: 10.22616/ERDev.2024.23.TF212. (indexed in Web of Science and Scopus).

P8 **B. S. Sadjiep Tchuigwa**, J. Krmela, J. Pokorn'y, and V. Krmelová, "Finite element modeling and analysis of tire creep test," in IOP Conference Series: Materials Science and Engineering, IOP Publishing, vol. 1319, 2024, p. 012 037.ISSN: 1757-899X, DOI: 10.1088/1757-899X/1319/1/012037. (indexed in Web of Science).

P9 J. Krmela, V. Krmelová, A. Artyukhov, **B. S. Sadjiep Tchuigwa**, and A. Bakošová, "Computational simulation of the shear test of a multi-layered long-fibre composite with a polymer matrix," IOP Conference Series: Materials Science and Engineering, vol. 1199, no. 1, p. 012 075, Nov. 2021, ISSN: 1757-899X, DOI: 10.1088/1757-899X/1199/1/012075. (indexed in Web of Science).

P10 J. Krmela, V. Krmelová, M. Gavendová, A. Bakošová, A Kasperovich, **B. S. Sadjiep Tchuigwa**, "Methods for determining the physico-mechanical properties of polymers". In petrochemistry–2020: proceedings. Minsk: Belarusian State Technological University, 2020. pp. 168-171 pp. ISBN 978-985-530-863-9. URL: Link.

Other publications: not related to the thesis

Journal paper: published

P11 P. Jilek, J. Berg, and **B. S. Sadjiep Tchuigwa**, "Influence of the weld joint position on the mechanical stress concentration in the construction of the alternative skid car system's skid chassis," Applied Sciences, vol. 12, no. 1, 2022, ISSN: 2076-3417. DOI: 2076-3417/12/1/397. **WoS Q3 (SCOPUS Q2/D2) Jimp**.

Conference proceedings : published

P12 J. Krmela, A. Bakosova, V. Krmelova, and **B. S. Sadjiep Tchuigwa**, "Drone propeller blade material optimization using modern computational method," in 20th International Scientific Conference Engineering for Rural Development Proceedings, Latvia University of Life Sciences and Technologies, Faculty of Engineering, May 2021, DOI: 10.22616/ERDev.2021.20.TF199. (indexed in Web of Science and Scopus).